

Search for narrow resonances in the dielectron and dimuon final states with CMS

Jordan TUCKER* for the CMS Collaboration

University of California, Los Angeles

E-mail: tucker@physics.ucla.edu

We describe the main results of a search with the CMS detector for narrow resonances in the dielectron and dimuon mass spectra using 1.1 fb^{-1} of pp collision data at $\sqrt{s} = 7 \text{ TeV}$ delivered by the LHC, highlighting the experimental challenges and differences between the two channels. Both the results of the resonant peak search and exclusion limits as a function of the mass of the new particle are presented.

XXIst International Europhysics Conference on High Energy Physics

21-27 July 2011

Grenoble, Rhône-Alpes France

*Speaker.

1. Introduction

New gauge bosons or other new particles, generically referred to here as Z' , decaying to pairs of electrons or muons could show up as a narrow resonant peak in the dilepton mass spectrum. We describe the main results of a search with the CMS detector for such Z' using 1.1 fb^{-1} of pp collision data at $\sqrt{s} = 7 \text{ TeV}$ delivered by the LHC. Details of the analysis can be found in [1].

We perform a generic shape-based search, making no assumptions on the absolute background rate. The results are normalized to the Standard Model (SM) Z^0 peak, using the ratio of cross sections (σ) times branching ratios (BR) into electrons or muons $R_\sigma = (\sigma \cdot \text{BR}(Z')) / (\sigma \cdot \text{BR}(Z^0))$. By normalizing to the Z^0 peak, several systematic effects cancel or are reduced in the ratio. For example, we avoid the uncertainty due to the absolute measurement of the luminosity. The absolute efficiencies also do not have to be exactly known, only how they evolve as a function of dilepton mass.

The CMS detector is described elsewhere [2]. Here we briefly highlight the different experimental issues for electrons and muons. The fine-grained electromagnetic calorimeter provides excellent dielectron mass resolution. The challenge, however, is on the identification of electrons versus the background from jets. On the other hand, muon identification is much easier, but the challenge is the dimuon mass resolution.

2. Dilepton selection and differences between the channels

The selection is simple: we require two good-quality isolated leptons. This selection is highly efficient: above 85% for dilepton masses above 1 TeV, mostly driven by the geometrical acceptance. As we normalize to the Z^0 cross section, the dilepton selection is almost the same as in that analysis, but adapted for high E_T/p_T leptons. Where there are differences, we account for them through small extra systematic uncertainties.

The main differences between the dielectron and dimuon channels are as follows. The dimuon channel suffers a smaller background due to muons from jets and misidentified muons, so the dimuon selection is a bit looser than that in the dielectron channel, leading to a slightly higher signal efficiency. Dimuons are required to be opposite-sign pairs, as the muon p_T measurement provided by the tracker is intrinsically linked to that of the muon charge.

The narrow peak from a new resonance is broadened by the dimuon mass resolution, driven by the muon momentum resolution. The dimuon channel, however, benefits from the studies of muon reconstruction performance using cosmic-ray events [3], especially in understanding the behavior of high- p_T muons that would originate from a potential Z' . This gives a handle on the resolution, confirming the reconstruction performance seen in simulation.

3. Dilepton backgrounds

The dominant, irreducible background is due to Drell-Yan (DY) dimuon production $Z^0/\gamma^* \rightarrow \ell^+\ell^-$; we use the shape of this background as predicted by the simulation in the peak search and limit setting.

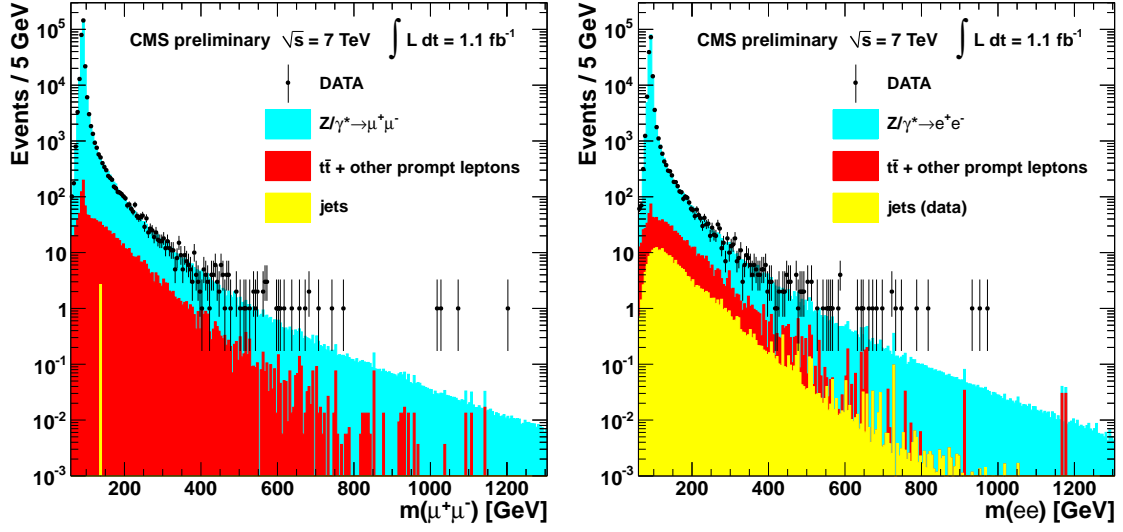


Figure 1: The invariant mass spectra of $\mu^+\mu^-$ (left) and ee (right) events. The points with error bars represent the data. The uncertainties on the data points (statistical only) represent 68% confidence intervals for the Poisson means. The filled histograms represent the expectations from SM processes: DY Z^0/γ^* , $t\bar{t}$, other sources of prompt leptons (tW , diboson production, $Z^0 \rightarrow \tau\tau$), and the backgrounds from misidentified jets.

Other, smaller sources of background are that from $t\bar{t}$ and other processes in which the leptons come from the decay of a W or a Z , referred to here as “prompt” leptons. The contributions from these processes total about 10% of the DY rate for dilepton masses above 120 GeV. To check this in the data, we exploit lepton universality, using $e\mu$ dileptons in data to predict the ee or $\mu\mu$ spectra from these sources; we find good agreement between the data and the simulation.

The dimuon background from misidentified jets is negligible, at a rate of less than 1% of DY above 120 GeV. As mentioned above, the dielectron channel suffers more from this background and is about 5% of the DY background in the same mass range. To estimate these backgrounds in data, we measure the probability for a jet to be reconstructed as an electron or muon with loosened cuts and to pass the rest of the selection. This provides an estimate of the contribution from jets to the dilepton spectra, which is compatible with the estimate from simulation.

4. The dilepton spectra, peak search, and mass limits

Figure 1 shows the dilepton mass spectra as observed in data overlaid on the SM prediction from simulation, with the various background processes separated into three main categories as described above. The histograms from the separate processes are normalized individually using the next-to-leading-order cross sections; the overall sum is then normalized to the data using the number of events around the Z^0 peak in the mass range from 60 to 120 GeV. To aid the comparison, Fig. 2 shows the cumulative distributions for data and simulation, the value in each bin being equal to the number of events having that mass or greater. There is good agreement between the data and the SM prediction.

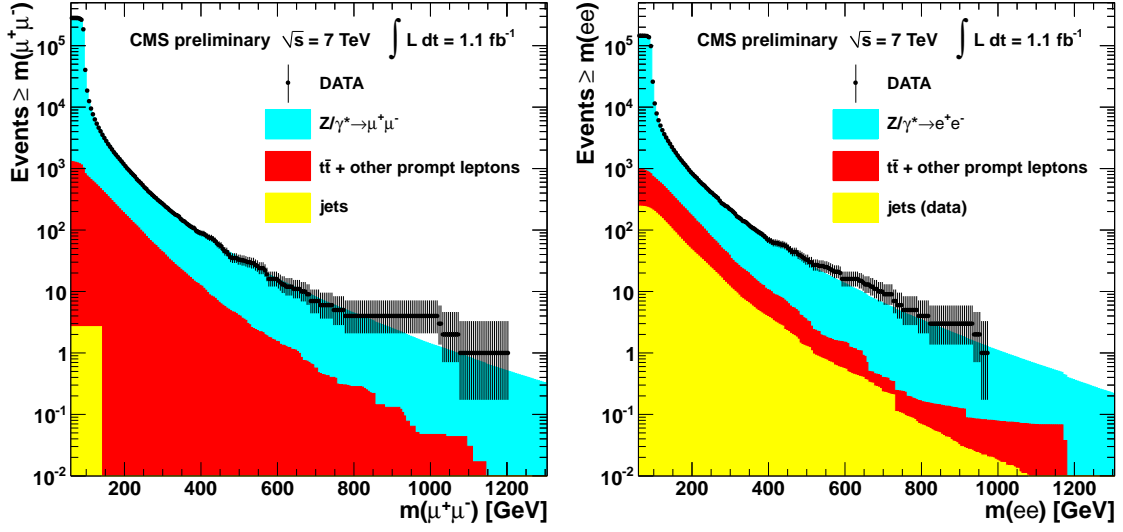


Figure 2: The cumulative distributions, starting from the high end, of the invariant mass spectra of $\mu^+\mu^-$ (left) and ee (right) events. The points with error bars represent the data, and the filled histograms represent the expectations from SM processes.

To quantify this agreement, we search for a resonance peak using unbinned maximum likelihood fits. This is done both separately for the dielectron and dimuon channels, and also for the combination of the two channels, taking the product of the individual likelihoods. In either channel, the likelihood uses a simple signal (Breit-Wigner convolved with a Gaussian) plus background (exponentially falling) probability density function. The fits then explore the difference in the shapes at every assumed Z' mass point M . The local significance is calculated using the likelihood ratio as $Z = \sqrt{2 \ln(L_{S+B}^{\max}/L_B)}$, where L_{S+B}^{\max} is the maximum likelihood under the signal plus background hypothesis, and L_B is the maximum likelihood for the background-only hypothesis. The largest local significances occur in the dielectron channel at 950 GeV with $Z = 2.2$, and in the dimuon channel at 1080 GeV with $Z = 1.7$; in the combination, the largest significance is at 970 GeV with $Z = 2.0$. Correcting for the probability of getting at least as extreme of a fluctuation from background-only in the range 600-2000 GeV (the “look-elsewhere effect”), the significances drop to 0.2, 0.3, and 0.2 in the dielectron, dimuon, and combination of channels, respectively.

We also set limits on the ratio of cross sections R_σ using a Bayesian method as a function of Z' mass M ; these limits are shown for the dielectron, dimuon, and combination of channels in Fig. 3. As benchmarks, we consider two Z' models [4], the sequential Standard Model Z_{SSM} and the superstring-inspired Z_ψ , and Randall-Sundrum massive gravitons [5] for two different values of the coupling parameter k/\bar{M}_{Pl} . For example, in the combination Z_ψ , the Z' with the smallest predicted cross section of those typically considered, is excluded at 95% C.L. for $M < 1620$ GeV.

5. Conclusion

We have conducted a search using the CMS detector for narrow resonances in the dielectron and dimuon channels using 1.1 fb^{-1} of pp collision data delivered by the LHC in the first half of

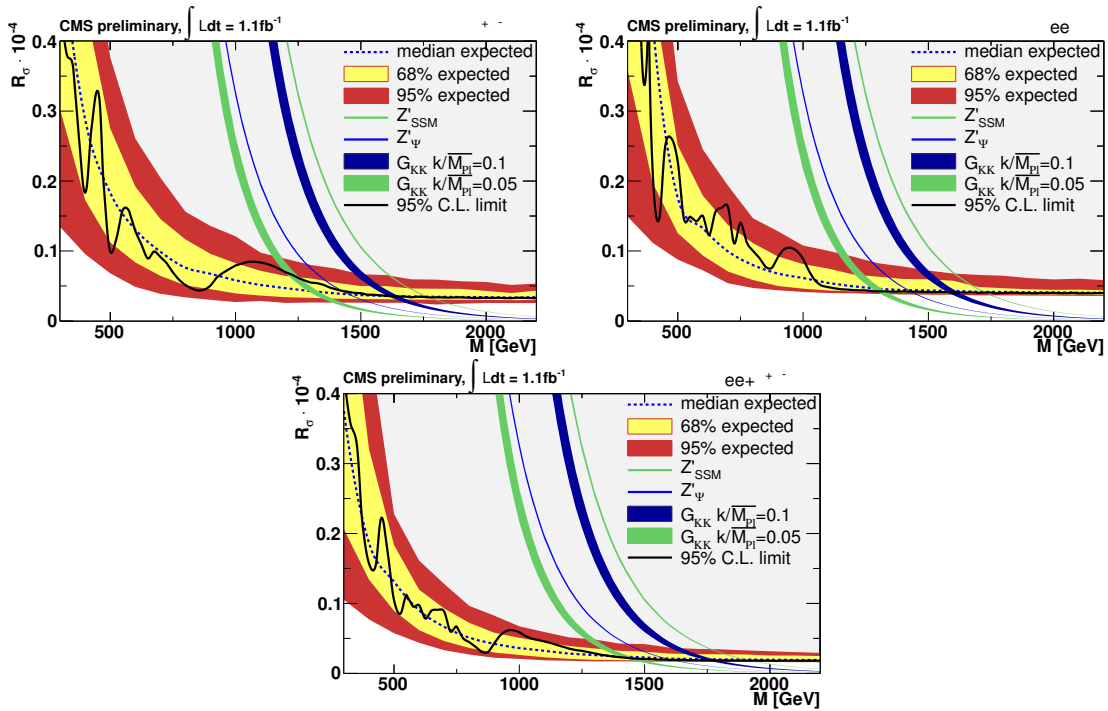


Figure 3: Upper limits on the ratio R_σ of cross section times branching fraction into lepton pairs, as a function of resonance mass M . The limits are shown from the $\mu^+\mu^-$ final state (top left), the ee final state (top right) and the combined dilepton result (bottom). The shaded yellow and red bands correspond to the 68% and 95% quantiles for the expected limits. The predicted cross section ratios for the benchmark models (Z_{SSM} , Z_ψ , and G_{KK} production) are shown as bands, with widths indicating the theoretical uncertainties.

2011. All cross-checks and systematic studies show that the detector is well understood and that the backgrounds are under control. We have begun to explore mass ranges well above that searched by the Tevatron, almost extending to $M = 2$ TeV. There is good agreement in the mass spectra between the data and the SM prediction, with no significant evidence for new particles observed.

References

- [1] S. Chatrchyan et al., *Search for resonances in the dilepton mass distribution in pp collisions at $\sqrt{s} = 7$ TeV*, CMS PAS EXO-11-019, <http://cdsweb.cern.ch/record/1369192>, 2011.
- [2] S. Chatrchyan et al., *The CMS experiment at the CERN LHC*, JINST **3** (2008) S08004.
- [3] S. Chatrchyan et al., *Performance of CMS muon reconstruction in cosmic-ray events*, JINST **5** (2010) T03022.
- [4] For a review, see e.g. P. Langacker, *The physics of heavy Z' gauge bosons*, Rev. Mod. Phys. **81** (2009) 1199.
- [5] L. Randall and R. Sundrum, *Large mass hierarchy from a small extra dimension*, Phys. Rev. Lett. **83** (1999) 3370.